Hindawi Publishing Corporation
International Journal of Photoenergy
Volume 2014, Article ID 197824, 7 pages
http://dx.doi.org/10.1155/2014/197824

Research Article

Synthesis, Characterization, and Photocatalytic Activity of Zn-Doped SnO_2/Zn_2SnO_4 Coupled Nanocomposites

Tiekun Jia,[1] Junwei Zhao,[1] Fang Fu,[1] Zhao Deng,[2] Weimin Wang,[2] Zhengyi Fu,[2] and Fancheng Meng[3]

[1] *Department of Materials Science and Engineering, Luoyang Institute of Science and Technology, Luoyang 471023, China*
[2] *State Key Lab of Materials Synthesis and Processing, Wuhan University of Technology, Wuhan 430070, China*
[3] *School of Materials Science and Engineering, Chongqing University of Technology, Chongqing 400050, China*

Correspondence should be addressed to Tiekun Jia; tiekunjia@126.com

Received 31 May 2013; Revised 8 November 2013; Accepted 11 November 2013; Published 28 January 2014

Academic Editor: Peter Robertson

Zn-doped SnO_2/Zn_2SnO_4 nanocomposites were prepared via a two-step hydrothermal synthesis method. The as-prepared samples were characterized by X-ray diffraction (XRD), field-emission scanning electron microscopy (FESEM), transmission electron microscopy (TEM), UV-vis diffuse reflection spectroscopy, and adsorption-desorption isotherms. The results of FESEM and TEM showed that the as-prepared Zn-doped SnO_2/Zn_2SnO_4 nanocomposites are composed of numerous nanoparticles with the size ranging from 20 nm to 50 nm. The specific surface area of the as-prepared Zn-doped SnO_2/Zn_2SnO_4 nanocomposites is estimated to be 71.53 m^2/g by the Brunauer-Emmett-Teller (BET) method. The photocatalytic activity was evaluated by the degradation of methylene blue (MB), and the resulting showed that Zn-doped SnO_2/Zn_2SnO_4 nanocomposites exhibited excellent photocatalytic activity due to their higher specific surface area and surface charge carrier transfer.

1. Introduction

Since the discovery of photoelectrochemical water splitting using TiO_2 electrodes [1], the investigation of the development of oxide semiconductor photocatalysts used for the degradation of environmental organic pollutants has attracted considerable attention for the past two decades [2–8]. Recently, Zn_2SnO_4 is considered to be a promising photocatalyst due to its high electron mobility, high electrical conductivity, and favorable stability in acidic and basic solutions [9–13]. It is reported that Zn_2SnO_4 nanostructures were used to decompose organic pollutants under UV light irradiation in previous studies [11, 12]. Ai et al. proposed a hydrothermal route to synthesize Zn_2SnO_4 microcubes and the photocatalytic activity of Zn_2SnO_4 microcubes was evaluated by the degradation of NO and HCHO under UV-vis light irradiation [11]. Tian et al. prepared Zn_2SnO_4 and Zn_2SnO_3 nanostructures by the combined strategy of laser ablation and hydrothermal treatment, and the results showed that Zn_2SnO_3 was active and effective for the degradation of methyl orange [12]. However, the fast recombination rate of the photogenerated electron/hole pairs of Zn_2SnO_4 prohibits the desirable photocatalytic activity. It is generally accepted that the technique of coupled oxides with different band gap widths is an effective approach to enhance the photocatalytic activity by increasing the separation of recombination rate of the photogenerated electron/hole pairs and extending the energy range of the photoexcitation [14–17]. Zn_2SnO_4 and SnO_2 have been investigated for the degradation of organic pollutants [11, 12, 18–21], and they have availably matched band gap widths for coupled composites [18, 19]. Additionally, the photocatalytic activity of SnO_2 can be enhanced by the zinc dopant ions incorporation into the lattice [20, 21]. Additionally, there are few reports on the synthesis and photocatalytic activity of Zn-doped SnO_2/Zn_2SnO_4.

Herein, we reported a two-step hydrothermal synthesis route for the preparation of Zn-doped SnO_2/Zn_2SnO_4 nanocomposites. The photocatalytic activity of the samples was evaluated by the degradation of MB, and the degradation process of MB was investigated in detail. To the best of

our knowledge, this is the first time to report the preparation and photocatalytic activity of Zn-doped SnO_2/Zn_2SnO_4 nanocomposites.

2. Experimental Details

2.1. Preparation of Zn-Doped SnO_2. The preparation of Zn-doped SnO_2 was also described in our previous studies [21]. All the reagents were analytically pure, purchased from Shanghai chemical industrial company, and used as received. In a typical procedure, 24 mmol NaOH was dissolved in 80 mL of mixed solvents containing 60% water and 40% ethanol. 3.43 mmol $SnCl_4{\cdot}5H_2O$ was added to the mixed solution under rigorous stirring. After constant stirring for 30 min, 0.57 mmol Zn $(NO_3)_2{\cdot}6H_2O$ was introduced into the mixed solution. After another 30 min of stirring, the obtained precursor was transferred into a 100 mL Teflon-lined stainless steel autoclave, and was put into an electric oven. The autoclave was maintained at 180°C for 20 h and cooled naturally to room temperature. The products were centrifuged and washed with distilled water and ethanol for several times, followed by drying in a vacuum oven at 60°C for 12 h.

2.2. Preparation of Zn-Doped SnO_2/Zn_2SnO_4. In a typical procedure, 2 mmol tin (IV) chloride pentahydrate ($SnCl_4{\cdot}5H_2O$) and 4 mmol zinc acetate dihydrate (Zn $(AC)_2{\cdot}2H_2O$) were dissolved in 20 mL mixed solvents of water and ethanol (volume ratio of 4 : 1) to form two transparent solutions, respectively. The above solutions were mixed together under magnetic stirring. A certain amount of the as-prepared Zn-doped SnO_2 was added into the mixed solution (Zn-doped SnO_2/Zn_2SnO_4 = 15 wt%). Then, 16 mmol sodium hydroxide (NaOH) was dissolved in 40 mL mixed solvents of water and ethanol (volume ratio of 4 : 1) to make a clear solution. In the next step, the NaOH solution was slowly dropped into the above mixed solution under magnetic stirring, and then the above solution was mixed by a magnetic stirrer for 1 hour. The obtained white suspension was transferred to Teflon-lined stainless steel autoclave with 100 mL capacity and heated at the temperature of 200°C for 15 h. After the autoclave had cooled naturally to room temperature, the final precipitates were centrifuged and washed with distilled water and ethanol, respectively, followed by drying under vacuum at 60°C for 12 h. Additionally, pure Zn_2SnO_4 was also obtained via a similar hydrothermal synthesis route without adding Zn-doped SnO_2.

2.3. Characterization. XRD pattern was carried out on a Rigaku ultima III diffraction meter equipped with Cu Kα radiation (λ = 0.15406 mn). FESEM images were taken using a Hitachi S-4800 field emission scanning electron microscope. TEM images were recorded on a JEM 2100 transmission electron microscope. The nitrogen adsorption and desorption isotherms at 77 K were measured using a Quantachrome NOVA 2000e sorption analyzer after samples were vacuum-dried at 473 K overnight. UV-vis diffuse reflectance spectra were recorded on a UV-vis spectrophotometer (UV2500, Shimadzu). The photoluminescence (PL) spectra were measured using a Hitachi F-4600 fluorescence spectrophotometer.

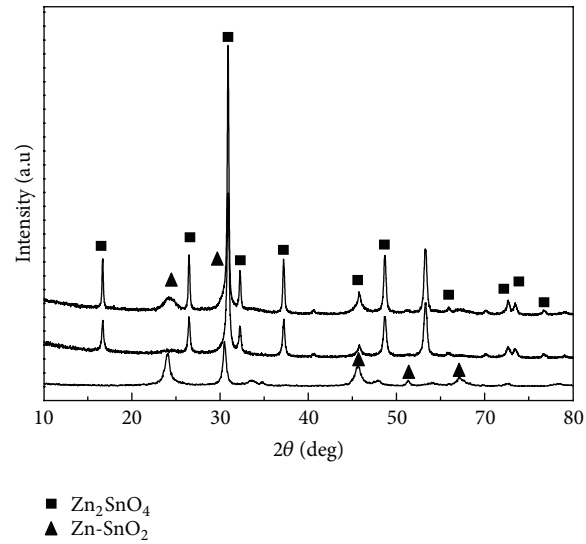

Figure 1: XRD patterns of as-prepared Zn-doped SnO_2, Zn_2SnO_4, and Zn-doped SnO_2/Zn_2SnO_4 nanocomposites.

2.4. Photocatalytic Experiments. The photocatalytic activity was evaluated by the decolorization of MB aqueous solution. As reported in our previous work [21, 22], 20 mL MB aqueous solution with a concentration of 1.0×10^{-5} M was added into the dish with 0.1 g prepared catalyst. A UV lamp (15 W, 365 nm) was used as light source to trigger the photocatalytic reaction. After irradiating for a certain time, the reacted solution was filtrated to measure the concentration variation of MB by recording the variation of the intensity of absorption peak centered at 664 nm using UV-visible spectrophotometer (UV-2550, Shimadzu, Japan). Consulting the literatures [23–25], the photodegradation efficiency of MB was evaluated by C/C_0, where C is concentration of the MB solution at reaction time t and C_0 is the adsorption/desorption equilibrium concentration of MB (at reaction time 0).

3. Results and Discussion

3.1. Phase and Morphology. XRD patterns of Zn-doped SnO_2, Zn_2SnO_4, and Zn-doped SnO_2/Zn_2SnO_4 nanocomposites are shown in Figure 1, respectively. From Figure 1, it can be found that the diffraction peaks in the pattern of Zn-doped SnO_2 are assigned to the tetragonal rutile structure of SnO_2 with lattice parameters comparable to the standard values (JCPDS, number 77-0451). Meanwhile, the characteristic peaks of Zn_2SnO_4 including (110), (220), (311), (222), (400), (422), (511), and (440) are in good accordance with the standard card of cubic Zn_2SnO_4 (JCPDS number 74-2184). For Zn-doped SnO_2/Zn_2SnO_4 nanocomposites, additional characteristic peaks with 2θ values of 26.36° and 33.86° appeared, which could be indexed to the (110) and (101)

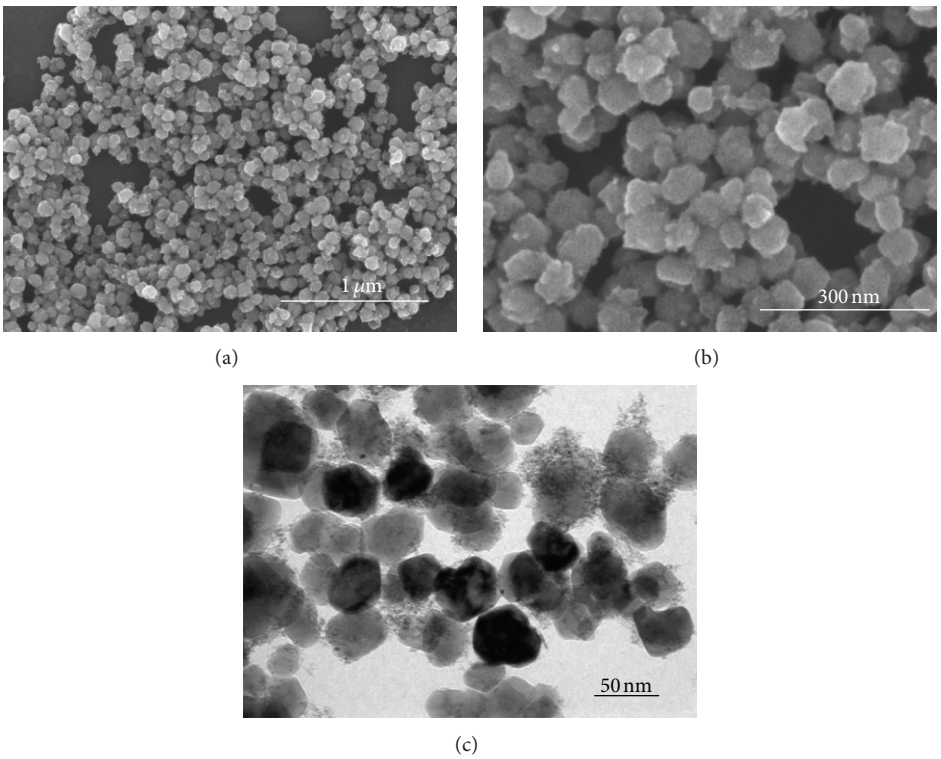

Figure 2: FESEM and TEM images of the Zn-doped SnO_2/Zn_2SnO_4 nanocomposites: (a) the panoramic FESEM image; (b) the high magnification FESEM image; and (c) TEM image.

crystal planes of SnO_2. No other impurities peaks are found in Zn-doped SnO_2/Zn_2SnO_4 nanocomposites, suggesting that the nanocomposites have a two-phase composition: Zn_2SnO_4 and Zn-doped SnO_2.

Figure 2 shows the FESEM and TEM images of Zn-doped SnO_2/Zn_2SnO_4 nanocomposites prepared via a two-step hydrothermal synthesis method. As seen in the typical FESEM image at low magnification (Figure 2(a)), the as-prepared Zn-doped SnO_2/Zn_2SnO_4 nanocomposites are composed of monodispersed and uniform nanoparticles. Figure 2(b) is the FESEM image at high magnification, which shows that the surfaces of the as-prepared Zn-doped SnO_2/Zn_2SnO_4 nanocomposites are rough. Furthermore, it is clearly observed that the size of the nanoparticles ranges from 25 nm to 50 nm from Figure 2(c), suggesting that the Zn-doped SnO_2/Zn_2SnO_4 nanocomposites might have larger surface area.

3.2. BET Surface Area and Pore Volume. The specific surface area and pore structure of the as-prepared Zn-doped SnO_2/Zn_2SnO_4 nanocomposites were investigated by nitrogen adsorption-desorption isotherm. Figure 3 shows the nitrogen adsorption-desorption isotherm with its pore size distribution in the inset. It is clear that the as-prepared Zn-doped SnO_2/Zn_2SnO_4 nanocomposites exhibit the type IV isotherm with type H3 hysteresis loop for the relative pressure P/P_0 in the range of 0.6–1 according to Brunauer-Deming-Deming-Teller (BDDT) classification [15, 26], revealing the characteristic of mesoporous materials and the presence of

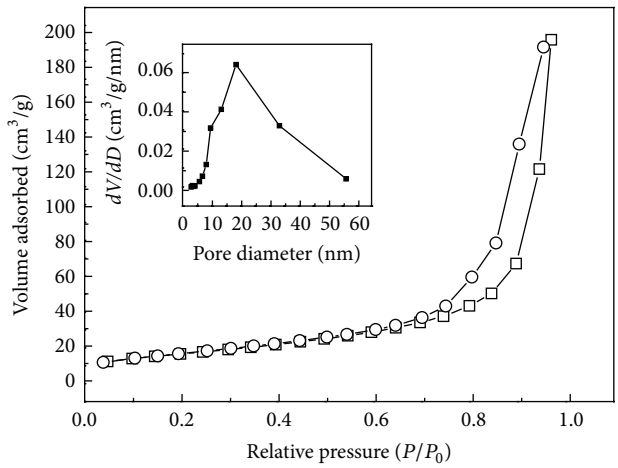

Figure 3: Nitrogen adsorption-desorption isotherm with its corresponding pore size distribution in the inset of the Zn-doped SnO_2/Zn_2SnO_4 nanocomposites.

mesopores (2–50 nm) [27]. The specific surface area estimated by Brunauer-Emmett-Teller method is 71.53 m^2/g. Furthermore, the observed hysteresis loop approaches $P/P_0 = 1$ indicating the presence of macropores (>50 nm) [27], which is in good agreement with the result of the corresponding pore size distribution of the sample in the inset of Figure 3. Additionally, the above macropores might result from the gaps between Zn-doped SnO_2/Zn_2SnO_4 nanoparticles.

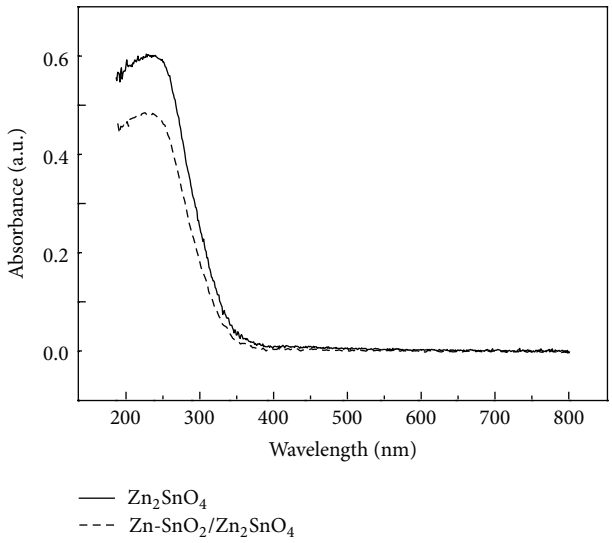

Figure 4: UV-vis absorbance spectra of pure Zn_2SnO_4 and Zn-doped SnO_2/Zn_2SnO_4 nanocomposites.

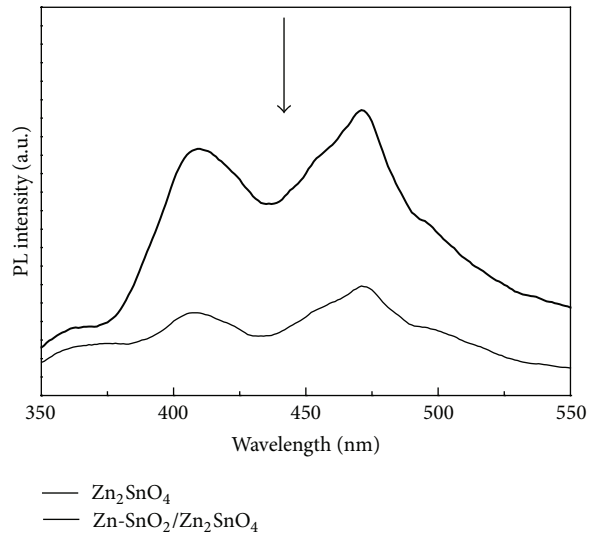

Figure 5: PL spectra of pure Zn_2SnO_4 and Zn-doped SnO_2/Zn_2SnO_4 nanocomposites.

3.3. UV-vis and PL Spectra. Figure 4 shows UV-vis absorbance spectra of pure Zn_2SnO_4 and Zn-doped SnO_2/Zn_2SnO_4 nanocomposites. The band gaps of pure Zn_2SnO_4 and Zn-doped SnO_2/Zn_2SnO_4 nanocomposites are estimated at 3.58 eV and 3.60 eV, respectively. The band gap of Zn-doped SnO_2/Zn_2SnO_4 nanocomposites is slightly higher than that of pure Zn_2SnO_4, which may be attributed to the synergistic effect of Zn-doped SnO_2 coupled with Zn_2SnO_4 homogeneous nanocomposites [28, 29].

To investigate the separation capacity of photogenerated carrier in nanocomposites, PL spectra of pure Zn_2SnO_4 and Zn-doped SnO_2/Zn_2SnO_4 nanocomposites were measured and the results are given in Figure 5. Two asymmetric peaks centered at 410 nm and 472 nm are observed from Figure 5, whereas the band to band emission peak (~360 nm) is not found in the curve. Consulting the literature [30, 31], the two peaks can be attributed to oxygen vacancies or surface states. It is also clear from Figure 5 that Zn-doped SnO_2/Zn_2SnO_4 nanocomposites exhibited lower emission intensity than that of pure Zn_2SnO_4 in the range of 400 nm and 500 nm. The above results reveal that the recombination of the photogenerated carriers in the composites decreased and a synergistic effect occurred between Zn-doped SnO_2 and Zn_2SnO_4 that favored the electron transfer [28, 29].

3.4. Photocatalytic Activity. Figure 6 presents the variations of adsorption spectra of aqueous MB in the presence of pure Zn_2SnO_4, Zn-doped SnO_2, and Zn-doped SnO_2/Zn_2SnO_4 nanocomposites under ultraviolet irradiation with the wavelength 365 nm. As seen in Figure 6(a), the intensity of the characteristic adsorption peak of MB at around 663 nm decreased with the irradiation time in the degradation process. Meanwhile, the color of the suspension faded away gradually with the irradiation time prolonging in the experiment. The characteristic adsorption peak disappeared, suggesting that the MB aqueous solution was degraded completely when the irradiation time reached 120 min. Figure 6(b) shows the photocatalytic performance of different photocatalysts with otherwise identical conditions under ultraviolet irradiation with the wavelength 365 nm. Blank test (MB without any catalyst) exhibited little photolysis. Meanwhile, the decrease of MB with Zn_2SnO_4 in the dark was similar to that of the blank test, which demonstrated that the adsorption of MB on the as-prepared photocatalysts was negligible after the adsorption-desorption equilibrium was reached. Additionally, the photocatalytic activities of pure Zn_2SnO_4 and Zn-doped SnO_2 were also performed to demonstrate the photocatalytic activity of Zn-doped SnO_2/Zn_2SnO_4. It is clear from Figure 6(b) that the Zn-doped SnO_2/Zn_2SnO_4 exhibited higher photocatalytic activities than that of pure Zn_2SnO_4 and pure Zn-doped SnO_2. Concerning the catalyst of pure Zn_2SnO_4, the complete degradation of MB was achieved when the irradiation time was 180 min.

It is well known that the augment of specific surface area and band gap is helpful for the improvement of photocatalytic activity [32–34]. In this experiment, pure Zn_2SnO_4 and Zn-doped SnO_2/Zn_2SnO_4 nanocomposites obtained via a similar hydrothermal synthesis route have similar specific surface area. Meanwhile, combined with the analysis of the UV-vis spectra, the value of the band gap of pure Zn_2SnO_4 is very close to that of Zn-doped SnO_2/Zn_2SnO_4 nanocomposites. Consequently, it can be inferred that surface area and band gap would have little effect on the photocatalytic performance of the above two catalysts. Based on the analysis, the enhanced photocatalytic activity can be explained as follows. The band gaps of Zn_2SnO_4 and Zn-doped SnO_2 have matched band potentials of coupling semiconductor. On the basis of the energy diagram reported in previous literature [10, 17–19], a proposed energy band structure diagram of the nanocomposites was elucidated schematically in Figure 7. Under UV light irradiation, Zn-doped SnO_2 and Zn_2SnO_4 would be excited simultaneously and generated electron-hole

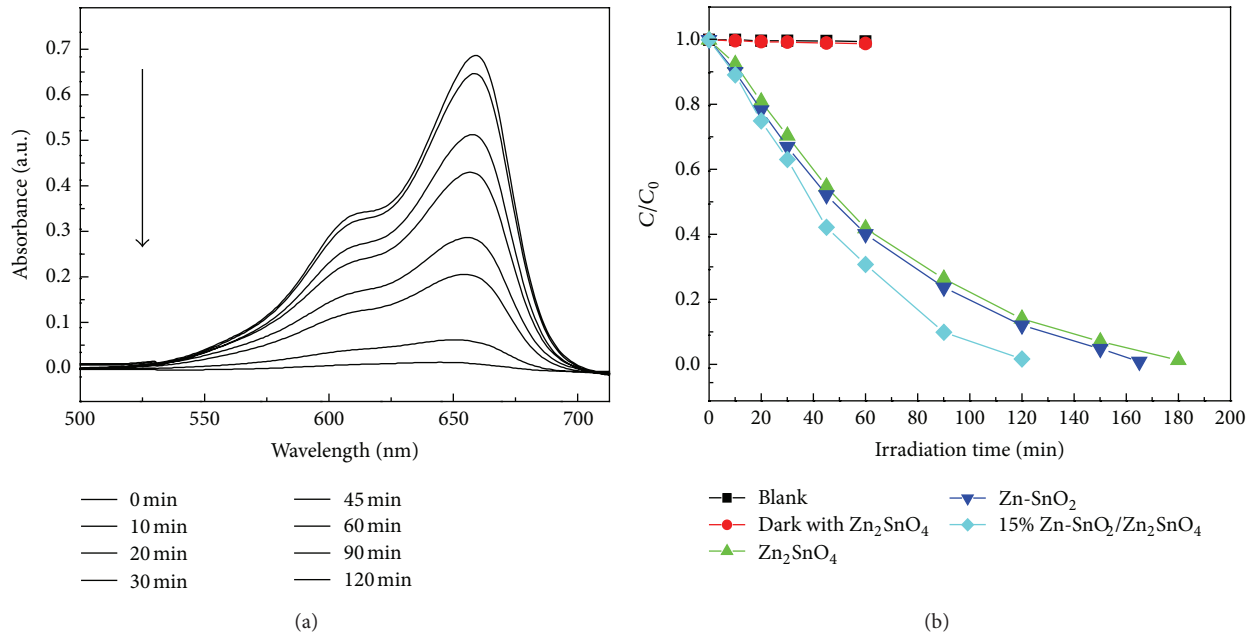

FIGURE 6: (a) The variations of adsorption spectra of aqueous MB in the presence of Zn-doped SnO_2/Zn_2SnO_4 nanocomposites at different periods of time under ultraviolet irradiation; (b) the comparisons of photocatalytic degradation activity of different photocatalysts, including pure Zn_2SnO_4, pure Zn-doped SnO_2, and 15% Zn-doped SnO_2/Zn_2SnO_4 nanocomposites.

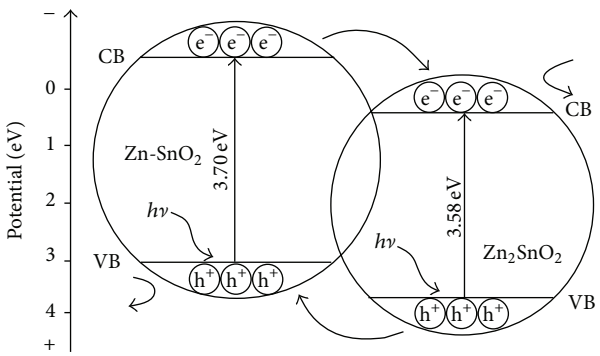

FIGURE 7: Schematic diagram for the illustration of the energy band structure and photogenerated electron hole pair separation in the Zn-doped SnO_2/Zn_2SnO_4 nanocomposites [10, 17–19].

pairs. As observed in Figure 7, the photogenerated electrons transfer occurred from CB of Zn-doped SnO_2 to the CB of Zn_2SnO_4 through the interface, whereas the photo-generated holes transfer occurred from VB of Zn_2SnO_4 to the VB of Zn-doped SnO_2 conversely, which led to the efficient separation of the photogenerated electrons and holes. Thus, the recombination rate of photoinduced charge carriers was suppressed significantly, which is also in good agreement with the result of PL spectra. Furthermore, the efficient charge separation could prolong the life time of the charge carriers and enhance the efficiency of the interfacial charge transfer to adsorbed substrates and then account for the higher photocatalytic activity of Zn-doped SnO_2/Zn_2SnO_4 nanocomposites. Additionally, it is noteworthy to be mentioned that the introduction of zinc ions is beneficial for the enhanced photocatalytic activity of the nanocomposites.

4. Conclusions

In summary, Zn-doped SnO_2/Zn_2SnO_4 nanocomposites were successfully prepared via a two-step hydrothermal synthesis route. The as-prepared nanocomposites are composed of numerous nanoparticles with the size ranging from 20 nm to 50 nm with higher specific surface area. The investigation of the photocatalytic activity indicated that the as-prepared Zn-doped SnO_2/Zn_2SnO_4 nanocomposites exhibit enhanced photocatalytic activities in the degradation of MB under UV light irradiation compared with that of pure Zn_2SnO_4, which is ascribed to the effective separation of photoinduced electron hole pairs.

Conflict of Interests

The authors declared that they do not have a direct financial relation with the commercial identities mentioned in this paper that might lead to any conflict of interests for any of the authors.

Acknowledgments

The authors express grateful thanks to the National Natural Science Foundation of China (Grants U1304520, 51102289, and 11204122) and the State Key Lab of Materials Synthesis and Processing of Wuhan University of Technology for the fund support.

References

[1] A. Fujishima and K. Honda, "Electrochemical photolysis of water at a semiconductor electrode," *Nature*, vol. 238, no. 5358, pp. 37–38, 1972.

[2] Z. Zou, J. Ye, K. Sayama, and H. Arakawa, "Direct splitting of water under visible light irradiation with an oxide semiconductor photocatalyst," *Nature*, vol. 414, no. 6864, pp. 625–627, 2001.

[3] R. Asahi, T. Morikawa, T. Ohwaki, K. Aoki, and Y. Taga, "Visible-light photocatalysis in nitrogen-doped titanium oxides," *Science*, vol. 293, no. 5528, pp. 269–271, 2001.

[4] J. Yu, Q. Xiang, and M. Zhou, "Preparation, characterization and visible-light-driven photocatalytic activity of Fe-doped titania nanorods and first-principles study for electronic structures," *Applied Catalysis B*, vol. 90, no. 3-4, pp. 595–602, 2009.

[5] X. Zhou, J. Shao, and B. Wan, "A one-step electrochemical method for the production of $TiO_{2-x}N_x$ nanotubes," *Journal of Electrochemical Society*, vol. 160, no. 6, pp. H335–H337, 2013.

[6] J. Qian, G. Cui, M. Jing, Y. Wang, M. Zhang, and J. Yang, "Hydrothermal synthesis of nitrogen-doped titanium dioxide and evaluation of its visible light photocatalytic activity," *International Journal of Photoenergy*, vol. 2012, Article ID 198497, 6 pages, 2012.

[7] J. Wei, B. Huang, P. Wang et al., "Photocatalytic properties of nitrogen-doped $Bi_{12}TiO_{20}$ synthesized by urea addition sol-gel method," *International Journal of Photoenergy*, vol. 2012, Article ID 135132, 8 pages, 2012.

[8] J. Zhang, Z. H. Hang, Y. Xu, and F. Kang, "Hydrothermal synthesis of iodine-doped Bi_2WO_6 nanoplates with enhanced visible and ultraviolet-induced photocatalytic activities," *International Journal of Photoenergy*, vol. 2012, Article ID 915386, 12 pages, 2012.

[9] M. A. Alpuche-Aviles and Y. Wu, "Photoelectrochemical study of the band structure of Zn_2SnO_4 prepared by the hydrothermal method," *Journal of the American Chemical Society*, vol. 131, no. 9, pp. 3216–3224, 2009.

[10] X. Y. Liu, H. W. Zheng, Z. L. Zhang, X. S. Liu, R. Q. Wan, and W. F. Zhang, "Effect of energy level matching on the enhancement of photovoltaic response about oxide/Zn_2SnO_4 composites," *Journal of Materials Chemistry*, vol. 21, pp. 4108–4116, 2011.

[11] Z. Ai, S. Lee, Y. Huang, W. Ho, and L. Zhang, "Photocatalytic removal of NO and HCHO over nanocrystalline Zn_2SnO_4 microcubes for indoor air purification," *Journal of Hazardous Materials*, vol. 179, no. 1–3, pp. 141–150, 2010.

[12] Z. Tian, C. Liang, J. Liu, H. Zhang, and L. Zhang, "Zinc stannate nanocubes and nanourchins with high photocatalytic activity for methyl orange and 2,5-DCP degradation," *Journal of Materials Chemistry*, vol. 22, no. 33, pp. 17210–17214, 2012.

[13] H. Zhu, D. Yang, G. Yu, H. Zhang, D. Jin, and K. Yao, "Hydrothermal synthesis of Zn_2SnO_4 nanorods in the diameter regime of sub-5 nm and their properties," *Journal of Physical Chemistry B*, vol. 110, no. 15, pp. 7631–7634, 2006.

[14] H. Wang, S. Baek, J. Lee, and S. Lim, "High photocatalytic activity of silver-loaded ZnO-SnO_2 coupled catalysts," *Chemical Engineering Journal*, vol. 146, no. 3, pp. 355–361, 2009.

[15] H. Yu, R. Liu, X. Wang, P. Wang, and J. Yu, "Enhanced visible-light photocatalytic activity of Bi_2WO_6 nanoparticles by Ag_2O cocatalyst," *Applied Catalysis B*, vol. 111-112, no. 28, pp. 326–333, 2012.

[16] J. Yu and J. Ran, "Facile preparation and enhanced photocatalytic H_2-production activity of $Cu(OH)_2$ cluster modified TiO_2," *Energy and Environmental Science*, vol. 4, no. 4, pp. 1364–1371, 2011.

[17] C. Wang, C. Shao, Y. Liu, and X. Li, "Water-dichloromethane interface controlled synthesis of hierarchical rutile TiO_2 superstructures and their photocatalytic properties," *Inorganic Chemistry*, vol. 48, no. 3, pp. 1105–1113, 2009.

[18] T. J. Coutts, D. L. Young, X. Li, W. P. Mulligan, and X. Wu, "Search for improved transparent conducting oxides: a fundamental investigation of CdO, Cd_2SnO_4, and Zn_2SnO_4," *Journal of Vacuum Science and Technology A*, vol. 18, no. 6, pp. 2646–2660, 2000.

[19] R. Könenkamp, R. C. Word, and M. Godinez, "Electroluminescence in nanoporous TiO_2 solid-state heterojunctions," *Nanotechnology*, vol. 17, no. 8, pp. 1858–1861, 2006.

[20] Z. Wen, G. Wang, W. Lu, Q. Wang, Q. Zhang, and J. Li, "Enhanced photocatalytic properties of mesoporous SnO_2 induced by low concentration ZnO doping," *Crystal Growth and Design*, vol. 7, no. 9, pp. 1722–1725, 2007.

[21] T. Jia, W. Wang, F. Long, Z. Fu, H. Wang, and Q. Zhang, "Synthesis, characterization, and photocatalytic activity of Zn-doped SnO_2 hierarchical architectures assembled by nanocones," *Journal of Physical Chemistry C*, vol. 113, no. 21, pp. 9071–9077, 2009.

[22] T. Jia, W. Wang, F. Long, Z. Fu, H. Wang, and Q. Zhang, "Fabrication, characterization and photocatalytic activity of La-doped ZnO nanowires," *Journal of Alloys and Compounds*, vol. 484, no. 1-2, pp. 410–415, 2009.

[23] H. Xu, Y. Xu, H. Li et al., "Synthesis, characterization and photocatalytic property of AgBr/$BiPO_4$ heterojunction photocatalyst," *Dalton Transactions*, vol. 41, no. 12, pp. 3387–3394, 2012.

[24] C. Pan and Y. Zhu, "Size-controlled synthesis of $BiPO_4$ nanocrystals for enhanced photocatalytic performance," *Journal of Materials Chemistry*, vol. 21, no. 12, pp. 4235–4241, 2011.

[25] M. Niu, F. Huang, L. Cui, P. Huang, Y. Yu, and Y. Wang, "Hydrothermal synthesis, structural characteristics, and enhanced photocatalysis of SnO_2/α-Fe_2O_3 semiconductor nanoheterostructures," *ACS Nano*, vol. 4, no. 2, pp. 681–688, 2010.

[26] S. Zhang, C. Zhang, Y. Man, and Y. Zhu, "Visible-light-driven photocatalyst of Bi_2WO_6 nanoparticles prepared via amorphous complex precursor and photocatalytic properties," *Journal of Solid State Chemistry*, vol. 179, no. 1, pp. 62–69, 2006.

[27] X. Wang, S. Li, H. Yu, and J. Yu, "In situ anion-exchange synthesis and photocatalytic activity of $Ag_8W_4O_{16}$/AgCl-nanoparticle core-shell nanorods," *Journal of Molecular Catalysis A*, vol. 334, no. 1-2, pp. 52–59, 2011.

[28] J. Shi, "On the synergetic catalytic effect in heterogeneous nanocomposite catalysts," *Chemical Reviews*, vol. 113, no. 3, pp. 2139–2181, 2013.

[29] F. T. Li, Y. Zhao, Y. J. Hao et al., "N-doped P25 TiO_2-amorphous Al_2O_3 composites: one-step solution combustion preparation and enhanced visible-light photocatalytic activity," *Journal of Hazardous Materials*, vol. 239-240, pp. 118–127, 2012.

[30] J. X. Wang, S. S. Xie, H. J. Yuan et al., "Synthesis, structure, and photoluminescence of Zn_2SnO_4 single-crystal nanobelts and nanorings," *Solid State Communications*, vol. 131, no. 7, pp. 435–440, 2004.

[31] X. Liu, J. Wang, E. Liang, and W. Zhang, "Enhancing mechanism of visible-light absorption for photovoltaic response and photoluminescence of Zn_2SnO_4 with high solubility of Bi^{3+}," *Applied Surface Science*, vol. 280, pp. 556–563, 2013.

[32] Y. Ohko, A. Fujishima, and K. Hashimoto, "Kinetic analysis of the photocatalytic degradation of gas-phase 2-propanol under mass transport-limited conditions with a TiO_2 film photocatalyst," *Journal of Physical Chemistry B*, vol. 102, no. 10, pp. 1724–1729, 1998.

[33] L. Cao, F. J. Spiess, A. Huang et al., "Heterogeneous photocatalytic oxidation of 1-butene on SnO_2 and TiO_2 films," *Journal of Physical Chemistry B*, vol. 103, no. 15, pp. 2912–2917, 1999.

[34] X. Song and L. Gao, "Fabrication of hollow hybrid microspheres coated with silica/titania via sol-gel process and enhanced photocatalytic activities," *Journal of Physical Chemistry C*, vol. 111, no. 23, pp. 8180–8187, 2007.